

Steepening and collapse in hydrodynamics and gasdynamics

N. A. Inogamov

L. D. Landau Institute of Theoretical Physics of the Russian Academy of Sciences, 117940 Moscow, Russia
(Submitted 23 January 1995)

Zh. Éksp. Teor. Fiz. **107**, 1596–1625 (May 1995)

The dynamics of a simply connected mass of liquid or gas bounded by a free surface is studied. Analytically (for the case of an incompressible liquid) and numerically (for the cases of incompressible liquids and gases with small values of the Mach number) it is shown that in the general formulation, starting from arbitrary initial data which are everywhere infinitely differentiable, singularities develop on this surface after a finite time in the course of evolution. Their occurrence is associated with the motion of singularities of the analytical continuation of the potential beyond the bounding free surface. It is found that in the process of the motion these singularities can approach the bounding surface and touch it. This is called hydrodynamic collapse. In the space–time neighborhood of the contact point the functional dependence of the variables steepens. As a result of collapse the bounding surface breaks up and a piece of a new free surface appears on it. Thereafter the bounding surface includes a bubble which expands into the interior of the fluid, and two spikes located at its edges. The bubble and the spikes separate from the singular point. The initial stages of this separation are self-similar. The piece of new surface is the surface of the bubble between the spikes. To put it another way, if the free surface was initially painted, then after a certain time unpainted regions of finite size appear on it. The spikes remain singular points on the bounding surface at which the spatial derivatives are singular for the entire infinite time of the subsequent evolution of the system. It is shown that this singular behavior does not depend on the presence or absence of a gravitational field. © 1995 American Institute of Physics.

1. INTRODUCTION

Self-steepening and collapse play an important role among problems that arise in investigations of nonlinear phenomena (see Refs. 1 and 2 and work cited therein). In this connection we recall, e.g., the breaking of Riemann waves³ and Langmuir collapse.^{4–6} In hydrodynamics there are several classes of problems related to steepening and concentration. Here it is worth recalling the broad class of cumulation problems, the vortex merging discovered by Aref,^{7,8} and singularities on fluid surfaces. Such singular behavior is frequently caused by the choice of initial conditions. For example, in connection with cumulation this behavior is due to the strict symmetry (e.g., spherical), while for vortex merging it is due to their special initial separation.¹ This is the origin of the important difference between the self-steepening regime studied in the present work with a broad class of capture determined by the initial data and these familiar examples.

In problems involving singularities at the surface of a liquid treatments have previously been published in which such singularities are associated with the crests of gravitational waves⁹ or liquid spikes for free fall in the absence of acceleration.^{1,2} In the present work collapse is observed with a completely new kind of singularity localization. Specifically, the peaks form not in the maxima of the liquid as in gravitational waves but rather in the troughs between the maxima. Furthermore, we are talking not about static features but about features that develop during the course of time. In problems involving singularities on a surface treatments are also well known in which the singularities are

already present on the surface initially. Examples include problems involving collisions of liquid or gas wedges or cones. The present work, however, is devoted to the study of the spontaneous development of collapse on a surface.

It is worth saying a few words about the physical assumptions under which the study of the surface dynamics of a liquid is of essential importance. Problems of current interest in physical hydrodynamics can be classified into internal and boundary. The former include turbulence of rotational fields in the bulk of the liquid, while the latter include turbulence near solid boundaries and the problem of the dynamics of a free surface treated in the present work.² The need for a detailed study of surface dynamics arises in many promising physical applications. It suffices to recall the Richtmyer–Meshkov, Kelvin–Helmholtz, and Rayleigh–Taylor instabilities in the physics of high energy densities (inertial fusion,^{10,11} the physics of explosions,^{12–14} ultrahigh magnetic fields,¹⁵ and other applications), astrophysics,^{16–18} and atmospheric and oceanic physics.¹⁹ (In this connection see also the reviews in Refs. 20 and 21.)

To conclude these introductory remarks we further note that in what follows we are primarily interested in cases in which the free-fall acceleration g is directed away from the liquid surface (Rayleigh–Taylor instability) or is absent (Richtmyer–Meshkov instability). For motions such as standing gravitational waves, when this acceleration is directed toward the liquid, singularities do not develop in the troughs for small ($v \ll \sqrt{g/k}$) and moderate ($v \approx \sqrt{g/k}$) amplitudes. For them to appear it is necessary that the initial velocities v be at least a factor of ten greater than the gravitational velocity $\sqrt{g/k}$. It is fairly obvious that for v

$\gg \sqrt{g/k}$ the case of standing gravitational waves in the initial part of the motion is close to the case of the Richtmyer–Meshkov instability.

2. STATEMENT OF THE PROBLEM

Consider the boundary-value problem specified by the following familiar^{3,22} kinematic and dynamic boundary conditions:

$$\eta_t = \varphi_y|_{\eta} - \eta_x \varphi_x|_{\eta}, \quad (1)$$

$$\varphi_t|_{\eta} = -v^2|_{\eta}/2 + g\eta, \quad (2)$$

where $y = \eta(x, t)$ defines the bounding surface and we have written $f_t \equiv \partial f / \partial t$, $f_x \equiv \partial f / \partial x$, φ is the potential ($\Delta\varphi=0$), $\mathbf{v} = \nabla\varphi$, $v^2 = \varphi_x^2 + \varphi_y^2$, $f|_{\eta} \equiv f(x, y = \eta, t)$, and the x and y axes are chosen so that only the y component of the acceleration g is nonzero. The liquid extends in the direction of negative y . The perturbations are localized in a layer at the surface [$\varphi(x, y \rightarrow -\infty, t) \rightarrow 0$] and fall off exponentially away from η . In the steady state $\partial_t = 0$ it follows from Eqs. (1) and (2) that the familiar^{3,22} boundary conditions for steady flow hold: $\varphi_y|_{\eta} = \eta_x \varphi_x|_{\eta}$ or $\psi|_{\eta} = 0$, where ψ is the stream function and $v^2|_{\eta} = 2g\eta$.

In hydromechanical applications this formulation applies to gravitational waves and to Rayleigh–Taylor and Richtmyer–Meshkov instabilities at surfaces. We have $g = -1$ in gravitational waves, $g = 1$ in the Rayleigh–Taylor instability, and $g = 0$ for the Richtmyer–Meshkov instability. The latter occurs when a shock wave passes through a density discontinuity.^{23,24} The shock wave starts perturbations growing with velocities $\sim cak$, where c is the speed of sound behind the wave front or the velocity of the wave itself (as is well known, these velocities are comparable), a is the initial perturbation amplitude, and k is the wave number. From the standpoint of fundamental investigations the most interesting case, as is usual for instabilities, is that in which initially linear perturbations grow. In this important limit the perturbations grow with velocities small compared to the speed of sound. The incompressible fluid approximation is therefore completely appropriate to describe the flow.

Let us consider the periodic case, when $\eta(x + 2\pi, t) = \eta(x, t)$ and $\varphi(x + 2\pi, y, t) = \varphi(x, y, t)$ hold. We use a system of units in which $|g| = k = 1$ holds to analyze the dynamics of the heavy fluid and $|v_0| = k = 1$ in the case of the Richtmyer–Meshkov instability; here v_0 is the amplitude of the initial velocity perturbation. In what follows we will approximate the Fourier expansions by truncating the series after a finite number of terms, and we will study the convergence of the results as a function of the harmonic number N . The truncated Fourier expansion of η takes the form

$$\eta = \sum_{n=1}^{N+1} \beta_n \cos(nx). \quad (3)$$

The constant β_0 vanishes because $\int_{-\infty}^{\infty} \eta(x, t) dx = M/\rho$ holds, where M and ρ are constants. The expansions of the complex potential f and its real part φ which satisfy the obvious symmetry and periodicity conditions and vanish at $y \rightarrow -\infty$ take the form

$$f(z, t) = \sum_{n=1}^N \frac{1}{n} \alpha_n(t) \exp(-inz),$$

$$\varphi(x, y, t) = \sum_{n=1}^N \frac{1}{n} \alpha_n(t) \cos(nx) \exp(ny), \quad (4)$$

where $z = x + iy$ and $\alpha_n(t)$ are real functions.

Let us discuss the relation that holds between the convergence of these expansions and the location of singularities of the potential. Consider the set of y -coordinates of these singularities. Let y_{down} be the smallest of these coordinates. The expansions (4) converge in the limit $N \rightarrow \infty$ if $y < y_{\text{down}}$ holds. This is because the asymptotic expressions for the Fourier amplitudes α_n in the limit $n \gg 1$ take the form

$$\alpha_n = \frac{c_1(n)}{c^n} = c_1(n) \exp(-ny_{\text{down}}), \quad (5)$$

where we have written $c = \exp(y_{\text{down}})$ and $c_1(n)$ is an amplitude whose growth in the limit $n \gg 1$ is bounded by some algebraic function.

We will study the result of substituting expansions (3), (4) into the boundary conditions (1), (2) and of expressing these conditions in terms of the amplitudes α_n and β_n .

3. THE EQUATIONS, THEIR INTEGRATION, AND THE RESULTS OF ANALYZING THE TRAJECTORIES

We begin with a brief description of how the equations will be derived. Writing φ in the form (4) satisfies the equation $\Delta\varphi=0$ and the conditions of periodicity, symmetry, and damping at infinity. It remains to deal with the boundary conditions (1), (2). Consider functions $K(x, y, t)$ and $D(x, y, t)$ of the form

$$K = \eta_t + \varphi_x \eta_x - \varphi_y, \quad D = \varphi_t + v^2/2 + p/\rho - gy.$$

Let us examine their behavior at the boundary. Set

$$\begin{aligned} k(x, t) &= K(x, y, t)|_{y=\eta(x, t)}, \\ d(x, t) &= D(x, y, t)|_{y=\eta(x, t)}. \end{aligned} \quad (6)$$

Now consider the functions $k(x, t)$ and $d(x, t)$, which are associated with the kinematic and boundary conditions, respectively, as can be seen from (1) and (2). From (1) and (2) it follows that the solutions of the problems satisfy $k = d = 0$ for all x . We regard k and d as functions of x . We expand them in Taylor series in x about the point x_{ac} , using k_n and d_n for the coefficients of the corresponding expansions. In terms of these coefficients the conditions $k = d = 0$ for all x imply $k_n = 0$, $d_n = 0$ to all orders in n . It remains to evaluate k_n and d_n as functions of α_n , β_n and $\dot{\alpha}_n$, $\dot{\beta}_n$. This gives rise to a system of ordinary differential equations. Let us now carry out this program.

3.1. Derivation of the dynamical system

The Fourier expansions (3), (4) with real amplitudes α_n and β_n describe spatially periodic solutions with alternating peaks and troughs (Fig. 1). By virtue of the symmetry under inversion in x it suffices to consider the half-period $0 \leq x \leq \pi$. The choice of the point x_{ac} in the half-period is important. For an arbitrary choice we obtain a differential

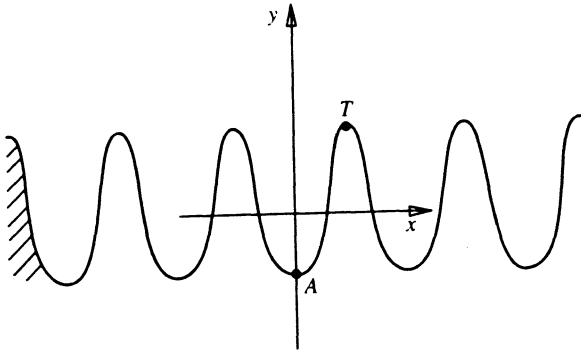


FIG. 1. Shape of the boundary $y = \eta(x, t)$. The liquid is indicated by hatching. A periodic sequence of crests and troughs is shown. The minimum point of η in the trough is indicated by the letter A and the top of the crest of the liquid by the letter T. In the text the laboratory and proper coordinate frames are important. The former is shown in this figure and the latter is attached to the point A.

system which approximates the boundary-value problem. We expand the conditions (1), (2) in Taylor series about the point A shown in Fig. 1, from which it follows that $x_{ac} = 0$. We discuss the basis for this choice and the closely related question of the interpretation of the results in Sec. 5.

In what follows we will need the power-series expansion of the function $\eta(x, t)$ about the point $x = 0$. We write this using the following notation:

$$\eta = \sum \eta_n(t) x^{2n}, \quad n = 0, 1, 2, \dots, N. \quad (7)$$

The coordinate system attached to the point A also plays an important role. In the laboratory system this point has coordinates $x = 0, y = \eta_0$ [see Eq. (7)]. The laboratory and proper coordinate systems are displaced by an amount η_0 equal to the displacement of the minimum of a trough (Fig. 1). The expansion (4) in the proper coordinates is equal to

$$F(Z, t) = \sum_{n=1}^N \frac{A_n(t)}{n} e^{-inZ} + i \dot{\eta}_0(t) Z, \quad (8)$$

$$\Phi(X, Y, t) = \sum_{n=1}^N \frac{A_n(t)}{n} \cos(nX) e^{nY} - \dot{\eta}_0(t) Y,$$

where we have written $F = \Phi + i\Psi$, $A_n = \alpha_n \exp(n\eta_0)$, and the relations $Z = z - i\eta_0, X = x, Y = y - \eta_0$ determine the passage from the laboratory (z) to the proper ($Z = X + iY$) coordinates. In the limit $Y \rightarrow -\infty$ the expansion (8) yields a uniform flow moving with velocity $\mathbf{V} = \nabla\Phi = (0, -\dot{\eta}_0)$.

Let us expand the function $k(X, t)$ given by Eq. (6) about the point $X = 0$. In view of the symmetry in the expansions of $k(X, t)$ and $d(X, t)$ only the even coefficients are nonzero. The expansion takes the form

$$k(X, t) = \sum k_n X^{2n} = \sum_{n=0}^N \dot{\eta}_n X^{2n} - \sum_{p,s=0} \frac{(-1)^p}{(2p+1)!s!} \left[2M_{2p+s+1} \sum_{m=1}^N m \eta_m X^{2m} \right.$$

$$\left. + (2p+1)M_{2p+s} \right] X^{2p} \left(\sum_{i=1}^N \eta_i X^{2i} \right)^s. \quad (9)$$

Expression (9) is found by substituting the Taylor series of the functions $\sin(nX), \cos(nX)$, and e^{nY} . Consequently, it is evident that the amplitudes A enter into Eq. (9) through the moments

$$M_i = \sum_{n=1}^N n^i A_n. \quad (10)$$

Multiplying the sums that appear in Eq. (9), transposing to the left-hand side terms containing derivatives with respect to t , and identifying successive powers of X^2 , after lengthy calculations we find the desired equations for $\dot{\eta}_n$ in the first seven orders of the expansion ($k_0 = 0, k_1 = 0, \dots, k_6 = 0$). These equations constitute half of the desired differential system (the other half gives equations for \dot{A}_n). They take the form

$$\begin{aligned} \dot{\eta}_0 &= M_0 \{1\}, \quad \dot{\eta}_1 = -M_2/2 + 3M_1\eta_1 \{2\}, \\ \dot{\eta}_2 &= \frac{M_4}{24} + 5 \left(-\frac{M_3\eta_1}{6} + \frac{M_2\eta_1^2}{2} + M_1\eta_2 \right) \{4\}, \\ \dot{\eta}_3 &= -\frac{M_6}{720} + 7 \left(\frac{M_5\eta_1}{120} - \frac{M_4\eta_1^2}{12} + \frac{M_3\eta_1^3}{6} - \frac{M_3\eta_2}{6} \right. \\ &\quad \left. + M_2\eta_1\eta_2 + M_1\eta_3 \right) \{7\}, \end{aligned} \quad (11)$$

$$\begin{aligned} \dot{\eta}_4 &= +\frac{M_8}{40320} - \frac{M_7\eta_1}{560} + \frac{3M_6\eta_1^2}{80} - \frac{M_5\eta_1^3}{4} - \dots \\ &\quad - \frac{3M_3\eta_3}{2} + 9M_2\eta_1\eta_3 + 9M_1\eta_4 \{12\}, \end{aligned}$$

$$\begin{aligned} \dot{\eta}_5 &= -\frac{M_{10}}{3628800} + 11 \left(\frac{M_9\eta_1}{362880} - \frac{M_8\eta_1^2}{10080} + \dots \right. \\ &\quad \left. - \frac{M_3\eta_4}{6} + M_2\eta_1\eta_4 + M_1\eta_5 \right) \{19\}, \end{aligned}$$

$$\begin{aligned} \dot{\eta}_6 &= \frac{M_{12}}{479001600} - 13 \left(\frac{M_{11}\eta_1}{39916800} + \dots + M_2\eta_2\eta_4 \right. \\ &\quad \left. - \frac{M_3\eta_5}{6} + M_2\eta_1\eta_5 + M_1\eta_6 \right) \{30\}; \end{aligned}$$

here and in what follows we use curly brackets to indicate the number of terms in the corresponding polynomial expressions.

Let us evaluate the equations for \dot{A}_n . They follow from the dynamic boundary condition $d(x, t) = 0$ [Eq. (6)] and the condition that the pressure $p(x, y, t)|_\eta = 0$ on the boundary be constant. The coefficients d_n consist of three components. They are the kinetic energy, the acceleration potential, and the gravitational potential. We list them here in order of decreasing computational complexity. Consider the first of these. Taking φ in the form (4), we calculate the components of $\nabla\varphi$, starting with $v^2|_\eta$. We express the amplitudes α_n in terms of A_n . As in the calculation of k_n we expand the cosine

and exponential functions in X and Y that enter into the resulting expression. After doing this we arrive at

$$v^2|_{\eta} = \sum_{p,s=0}^N \sum_{n,m=1}^N \frac{(-1)^p (n-m)^{2p} (n+m)^s}{(2p)! s!} A_n A_m X^{2p} \times \left(\sum_{i=1}^N \eta_m X^{2m} \right)^s.$$

Then we raise $(n \pm m)$ to the appropriate power and multiply the resulting series. We eliminate the summation over n and m by means of the expressions (10) for the moments. As a result the moments M_n enter into the equations instead of the amplitudes A_n , and the equations themselves acquire a more compact form. The final expressions, prepared for expansion in X^2 , assume the form

$$v^2|_{\eta} = \sum_{p,s=0}^{2p} \sum_{i=0}^s \sum_{j=0}^s \frac{(-1)^{p+i} M(i+j) M(2p+s-i-j)}{i! j! (2p-i)! (s-j)!} X^{2p} \times \left(\sum_{i=1}^N \eta_m X^{2m} \right)^s. \quad (12)$$

Here for simplicity we have written M_n as $M(n)$.

Now we calculate the acceleration potential. We perform the calculation in the laboratory coordinate frame and then express $\dot{\alpha}_n$ in terms of A_n and \dot{A}_n using the formula $\dot{\alpha}_n = (\dot{A}_n - n \dot{\eta}_0 A_n) \exp(-n \eta_0)$. We eliminate $\dot{\eta}_0$ using the first equation of the subsystem (11). Going over to moments we find

$$\varphi_i|_{\eta} = \sum_{p,s=0}^N \frac{(-1)^p [M(2p+s-1) - M(0)M(2p+s)]}{(2p)! s!} \times X^{2p} \left(\sum_{i=1}^N \eta_m X^{2m} \right)^s. \quad (13)$$

Now we have everything necessary to derive the second half of this system. Substituting Eqs. (12) and (13) and the expression for the gravitational potential, which is proportional to (7), into $d(X,t)$ and expanding $d(X,t)$ in a Taylor series and collecting the time derivatives on the left-hand side of the equations, we find in the first seven orders of the expansion

$$\begin{aligned} \dot{M}_{-1} &= \frac{M_0^2}{2} + g \eta_0 \quad \{1,2\}, \\ -\frac{\dot{M}_1}{2} + \dot{M}_0 \eta_1 &= -\frac{M_1^2}{2} + g \eta_1 \quad \{2,2\}, \\ \frac{\dot{M}_3}{24} - \frac{\dot{M}_2 \eta_1}{2} + \frac{\dot{M}_1 \eta_1^2}{2} + \dot{M}_0 \eta_2 &= -\frac{M_2^2}{8} + \frac{M_1 M_3}{6} \\ &\quad - \frac{M_1 M_2 \eta_1}{2} - \frac{M_1^2 \eta_1^2}{2} + g \eta_2 \quad \{4,5\}, \quad -\frac{\dot{M}_5}{720} \\ &\quad + \frac{\dot{M}_4 \eta_1}{24} - \frac{\dot{M}_3 \eta_1^2}{4} + \frac{\dot{M}_2 \eta_1^3}{6} - \frac{\dot{M}_2 \eta_2}{2} + \dot{M}_1 \eta_1 \eta_2 \end{aligned}$$

$$\begin{aligned} + \dot{M}_0 \eta_3 &= -\frac{M_3^2}{72} + \frac{M_2 M_4}{48} - \frac{M_1 M_5}{120} - \frac{M_2 M_3 \eta_1}{12} \\ &\quad - \dots - \frac{M_1 M_2 \eta_2}{2} - M_1^2 \eta_1 \eta_2 + g \eta_3 \quad \{7,10\}, \end{aligned} \quad (14)$$

$$\begin{aligned} \frac{\dot{M}_7}{40320} - \frac{\dot{M}_6 \eta_1}{720} + \frac{\dot{M}_5 \eta_1^2}{48} - \frac{\dot{M}_4 \eta_1^3}{12} + \dots + \frac{\dot{M}_1 \eta_2^2}{2} \\ - \frac{\dot{M}_2 \eta_3}{2} + \dot{M}_1 \eta_1 \eta_3 + \dot{M}_0 \eta_4 &= -\frac{M_4^2}{1152} + \frac{M_3 M_5}{720} \\ - \frac{M_2 M_6}{1440} + \frac{M_1 M_7}{5040} + \dots - M_1^2 \eta_1 \eta_3 \\ + g \eta_4 \quad \{12,22\}, \quad -\frac{\dot{M}_9}{3628800} + \frac{\dot{M}_8 \eta_1}{40320} \\ - \frac{\dot{M}_7 \eta_1^2}{1440} - \dots + \dot{M}_1 \eta_2 \eta_3 - \frac{\dot{M}_2 \eta_4}{2} + \dot{M}_1 \eta_1 \eta_4 \\ + \dot{M}_0 \eta_5 &= -\frac{M_5^2}{28800} + \frac{M_4 M_6}{17280} - \frac{M_3 M_7}{30240} + \dots \\ - M_1^2 \eta_2 \eta_3 - \frac{M_1 M_2 \eta_4}{2} - M_1^2 \eta_1 \eta_4 \\ + g \eta_5 \quad \{19,41\}, \\ \frac{\dot{M}_{11}}{479001600} - \frac{\dot{M}_{10} \eta_1}{3628800} + \frac{\dot{M}_9 \eta_1^2}{80640} + \dots + \dot{M}_1 \eta_2 \eta_4 \\ - \frac{\dot{M}_2 \eta_5}{2} + \dot{M}_1 \eta_1 \eta_5 + \dot{M}_0 \eta_6 &= -\frac{M_6^2}{1036800} \\ + \frac{M_5 M_7}{604800} - \frac{M_4 M_8}{967680} + \frac{M_3 M_9}{2177280} - \dots \\ + g \eta_6 \quad \{30,72\}. \end{aligned}$$

Here the pairs of numbers in braces represent the number of terms on the left- and right-hand sides of the corresponding equations. Note that the first equation in this subsystem should be omitted. The point is that it corresponds to the zeroth order in the expansion of $d(X,t)$, while the boundary condition $d(X,t)=0$ holds (as is well known) only to within an arbitrary homogeneous function of time. Note also that the first equation in the subsystem (11) can be integrated after the other equations in the system (11), (14), since the unknown function η_0 does not enter there. Consequently, for $N=6$ we must integrate six equations simultaneously from the subsystem (11) and six equations from the subsystem (14); for $N=5$ there are ten of these simultaneously integrated equations, and so on. To derive systems of lower order it is necessary to omit the corresponding higher-order equations in the subsystems (11) and (14).

Let us express the system (11), (14) in terms of the amplitudes A_n . For this we substitute for M_n using Eq. (10). After lengthy calculations we reduce the differential system to the following form:

$$\dot{A}_i = \sum_{j=1}^N (G^{-1})_{ij} \left(g \eta_j + \sum_{k,m=1}^N M_{jkm} A_k A_m \right), \quad (15)$$

$$\dot{\eta}_i = \sum_{j=1}^N D_{ij} A_j, \quad (16)$$

$i = 1, 2, \dots, N$, and the matrix elements of the two- and three-dimensional matrices G , M , and D are polynomial functions only of the boundary surface function $\eta(x, t)$ specified by the quantities η_1, \dots, η_N . We start by giving the equations for G and D . They take the form

$$G_{11} = -\frac{1}{2} - \eta_1, \quad G_{12} = -1 - \eta_1, \quad G_{13} = -\frac{3}{2} - \eta_1,$$

$$G_{14} = -2 - \eta_1, \quad G_{15} = -\frac{5}{2} - \eta_1, \quad G_{16} = -3 - \eta_1,$$

$$G_{21} = \frac{1}{24} + \frac{\eta_1}{2} + \frac{\eta_1^2}{2} - \eta_2, \quad G_{22} = \frac{1}{3} + 2\eta_1 + \eta_1^2 - \eta_2,$$

$$G_{23} = \frac{9}{8} + \frac{9\eta_1}{2} + \dots, \quad G_{24} = \frac{8}{3} + 8\eta_1 + \dots,$$

$$G_{25} = \frac{125}{24} + \frac{25\eta_1}{2} + \dots, \quad G_{26} = 9 + 18\eta_1 + \dots,$$

$$G_{31} = -\frac{1}{720} - \frac{\eta_1}{24} - \frac{\eta_1^2}{4} - \frac{\eta_1^3}{6} + \frac{\eta_2}{2} + \eta_1\eta_2 - \eta_3,$$

$$G_{32} = -\frac{2}{45} - \frac{2\eta_1}{3} - \dots, \quad G_{33} = -\frac{27}{80} - \frac{27\eta_1}{8} - \dots,$$

$$G_{34} = -\dots, \quad G_{35} = -\dots, \quad G_{36} = -\dots,$$

$$G_{41} = \frac{1}{40320} + \frac{\eta_1}{720} + \frac{\eta_1^2}{48} + \frac{\eta_1^3}{12} + \frac{\eta_1^4}{24} - \frac{\eta_2}{24} - \frac{\eta_1\eta_2}{2} - \frac{\eta_1^2\eta_2}{2} + \frac{\eta_2^2}{2} + \frac{\eta_3}{2} + \eta_1\eta_3 - \eta_4,$$

$$G_{42} = \frac{1}{315} + \frac{4\eta_1}{45} + \dots, \quad G_{43} = \frac{243}{4480} + \frac{81\eta_1}{80} + \dots,$$

$$G_{44} = \dots, \quad G_{45} = \dots, \quad G_{46} = \dots,$$

$$G_{51} = -\frac{1}{3628800} - \frac{\eta_1}{40320} - \frac{\eta_1^2}{1440} - \frac{\eta_1^3}{144} - \frac{\eta_1^4}{48} - \frac{\eta_1^5}{120} + \frac{\eta_2}{720} + \frac{\eta_1\eta_2}{24} + \frac{\eta_1^2\eta_2}{4} + \frac{\eta_1^3\eta_2}{6} - \frac{\eta_2^2}{4} - \frac{\eta_1\eta_2^2}{2} - \frac{\eta_3}{24} - \frac{\eta_1\eta_3}{2} - \frac{\eta_1^2\eta_3}{2} + \eta_2\eta_3 + \frac{\eta_4}{2} + \eta_1\eta_4 - \eta_5,$$

$$G_{52} = -\frac{2}{14175} - \dots, \quad G_{53} = -\frac{243}{44800} - \dots,$$

$$G_{54} = -\dots, \quad G_{55} = -\dots, \quad G_{56} = -\dots,$$

$$G_{61} = \frac{1}{479001600} + \frac{\eta_1}{3628800} + \frac{\eta_1^2}{80640} + \frac{\eta_1^3}{4320} + \frac{\eta_1^4}{576} + \frac{\eta_1^5}{240} + \frac{\eta_1^6}{720} - \frac{\eta_2}{40320} - \frac{\eta_1\eta_2}{720} - \frac{\eta_1^2\eta_2}{48} - \frac{\eta_1^3\eta_2}{12} - \frac{\eta_1^4\eta_2}{24} + \frac{\eta_2^2}{48} + \frac{\eta_1\eta_2^2}{4} + \frac{\eta_1^2\eta_2^2}{4} - \frac{\eta_2^3}{6} + \frac{\eta_3}{720} + \frac{\eta_1\eta_3}{24} + \frac{\eta_1^2\eta_3}{4} + \frac{\eta_1^3\eta_3}{6} - \frac{\eta_2\eta_3}{2} - \eta_1\eta_2\eta_3 + \frac{\eta_2^2}{2} - \frac{\eta_4}{24} - \frac{\eta_1\eta_4}{2} - \frac{\eta_1^2\eta_4}{2} + \eta_2\eta_4 + \frac{\eta_5}{2} + \eta_1\eta_5 - \eta_6,$$

$$G_{62} = \frac{2}{467775} + \frac{4\eta_1}{14175} + \dots, \quad G_{63} = \frac{729}{1971200} + \dots, \quad G_{64} = \dots, \quad G_{65} = \dots, \quad G_{66} = \dots,$$

$$D_{11} = \frac{1}{2} + 3\eta_1, \quad D_{12} = 2 + 6\eta_1, \quad D_{13} = \frac{9}{2} + 9\eta_1,$$

$$D_{14} = 8 + 12\eta_1, \quad D_{15} = \frac{25}{2} + 15\eta_1, \quad D_{16} = 18 + 18\eta_1,$$

$$D_{21} = -\frac{1}{24} - \frac{5\eta_1}{6} - \frac{5\eta_1^2}{2} + 5\eta_2, \quad D_{22} = -\frac{2}{3} - \frac{20\eta_1}{3} - 10\eta_1^2 + 10\eta_2,$$

$$D_{23} = -\frac{27}{8} - \frac{45\eta_1}{2} - \frac{45\eta_1^2}{2} + 15\eta_2, \quad D_{24} = -\frac{32}{3} - \frac{160\eta_1}{3} - 40\eta_1^2 + 20\eta_2,$$

$$D_{25} = -\frac{625}{24} - \frac{625\eta_1}{6} - \frac{125\eta_1^2}{2} + 25\eta_2, \quad D_{26} = -54 - 180\eta_1 - 90\eta_1^2 + 30\eta_2,$$

$$D_{31} = \frac{1}{720} + \frac{7\eta_1}{120} + \frac{7\eta_1^2}{12} + \frac{7\eta_1^3}{6} - \frac{7\eta_2}{6} - 7\eta_1\eta_2 + 7\eta_3,$$

$$D_{32} = \frac{4}{45} + \frac{28\eta_1}{15} + \dots, \quad D_{33} = \frac{81}{80} + \dots, \quad D_{34} = \dots, \quad D_{35} = \dots, \quad D_{36} = \dots,$$

$$D_{41} = -\frac{1}{40320} - \frac{\eta_1}{560} - \frac{3\eta_1^2}{80} - \frac{\eta_1^3}{4} - \frac{3\eta_1^4}{8} + \frac{3\eta_2}{40} + \frac{3\eta_1\eta_2}{2} + \frac{9\eta_1^2\eta_2}{2} - \frac{9\eta_2^2}{2} - \frac{3\eta_3}{2} - 9\eta_1\eta_3 + 9\eta_4,$$

$$D_{42} = -\frac{2}{315} - \dots, \quad D_{43} = -\frac{729}{4480} - \dots,$$

$$D_{44} = -\dots, \quad D_{45} = -\dots, \quad D_{46} = -\dots,$$

$$D_{51} = \frac{1}{3628800} + 11 \left(\frac{\eta_1}{362880} + \frac{\eta_1^2}{10080} + \frac{\eta_1^3}{720} + \frac{\eta_1^4}{144} + \frac{\eta_1^5}{120} - \frac{\eta_2}{5040} - \frac{\eta_1 \eta_2}{120} - \frac{\eta_1^2 \eta_2}{12} - \frac{\eta_1^3 \eta_2}{6} + \frac{\eta_2^2}{12} + \frac{\eta_1 \eta_2^2}{2} + \frac{\eta_3}{120} + \frac{\eta_1 \eta_3}{6} + \frac{\eta_1^2 \eta_3}{2} - \eta_2 \eta_3 - \frac{\eta_4}{6} - \eta_1 \eta_4 + \eta_5 \right),$$

$$D_{52} = \frac{4}{14175} + \dots, \quad D_{53} = \frac{729}{44800} + \dots, \quad D_{54} = \dots,$$

$$D_{55} = \dots, \quad D_{56} = \dots,$$

$$D_{61} = -\frac{1}{479001600} + 13 \left(-\frac{\eta_1}{39916800} - \frac{\eta_1^2}{725760} - \frac{\eta_1^3}{30240} - \frac{\eta_1^4}{2880} - \frac{\eta_1^5}{720} - \frac{\eta_1^6}{720} + \frac{\eta_2}{362880} + \frac{\eta_1 \eta_2}{5040} + \frac{\eta_1^2 \eta_2}{240} + \frac{\eta_1^3 \eta_2}{36} + \frac{\eta_1^4 \eta_2}{24} - \frac{\eta_2^2}{240} - \frac{\eta_1 \eta_2^2}{12} - \frac{\eta_1^2 \eta_2^2}{4} + \frac{\eta_2^3}{6} - \frac{\eta_3}{5040} - \frac{\eta_1 \eta_3}{120} - \frac{\eta_1^2 \eta_3}{12} - \frac{\eta_1^3 \eta_3}{6} + \frac{\eta_2 \eta_3}{6} + \eta_1 \eta_2 \eta_3 - \frac{\eta_2^2}{2} + \frac{\eta_4}{120} + \frac{\eta_1 \eta_4}{6} + \frac{\eta_1^2 \eta_4}{2} - \eta_2 \eta_4 - \frac{\eta_5}{6} - \eta_1 \eta_5 + \eta_6 \right)$$

$$D_{62} = -\frac{4}{467775} - \dots, \quad D_{63} = -\frac{2187}{1971200} - \dots,$$

$$D_{64} = -\dots, \quad D_{65} = -\dots, \quad D_{66} = -\dots$$

In writing these expressions we have tried to standardize their information content. Analysis of the expressions G_{ij} and D_{ij} reveals that the structure of the polynomials changes only from one column to the next. Within a column only the coefficients for the corresponding terms change. We have also tried to make the notation compact. Consequently, we have given complete expressions for the first elements in a column, and have written the others where necessary with ellipses.

Now we write down expressions for the matrices M_{ijk} associated with the kinetic energy. They take the form

$$M(111) = -\frac{1}{2}, \quad M(112) = -2, \quad M(113) = -3,$$

$$M(114) = -4, \quad M(115) = -5, \dots,$$

$$M(155) = -\frac{25}{2}, \quad M(156) = -30, \quad M(166) = -18,$$

$$M(211) = \frac{1}{24} + \frac{\eta_1}{2} - \frac{\eta_1^2}{2}, \quad M(212) = \frac{2}{3} + 3\eta_1 - 2\eta_1^2, \dots,$$

$$M(255) = 625/24 + \dots, \quad M(256) = \dots, \quad M(266) = \dots,$$

$$M(311) = -\frac{1}{720} - \frac{\eta_1}{24} - \frac{\eta_1^2}{4} + \frac{\eta_1^3}{2} + \frac{\eta_2}{2} - \eta_1 \eta_2,$$

$$M(312) = -\dots, \dots,$$

$$M(356) = -\frac{173}{2} - \frac{1815 \eta_1}{4} - \dots, \quad M(366) = -\frac{324}{5} - \dots,$$

$$M(411) = \frac{1}{40320} + \frac{\eta_1}{720} + \frac{\eta_1^2}{48} + \frac{\eta_1^3}{12} - \frac{7\eta_1^4}{24} - \frac{\eta_2}{24} - \frac{\eta_1 \eta_2}{2} + \frac{3\eta_1^2 \eta_2}{2} - \frac{\eta_2^2}{2} + \frac{\eta_3}{2} - \eta_1 \eta_3,$$

$$M(412) = \frac{2}{315} + \dots, \dots, \quad M(455) = \dots,$$

$$M(456) = \dots, \quad M(466) = \dots,$$

$$M(511) = -\frac{1}{3628800} - \frac{\eta_1}{40320} - \frac{\eta_1^2}{1440} - \frac{\eta_1^3}{144} - \frac{\eta_1^4}{48} + \frac{\eta_1^5}{8} + \frac{\eta_2}{720} + \frac{\eta_1 \eta_2}{24} + \frac{\eta_1^2 \eta_2}{4} - \frac{7\eta_1^3 \eta_2}{6} - \frac{\eta_2^2}{4} + \frac{3\eta_1 \eta_2^2}{2} - \frac{\eta_3}{24} - \frac{\eta_1 \eta_3}{2} + \frac{3\eta_1^2 \eta_3}{2} - \eta_2 \eta_3 + \frac{\eta_4}{2} - \eta_1 \eta_4,$$

$$M(512) = -\frac{4}{14175} - \dots, \quad M(513) = -\dots,$$

$$M(514) = -\dots, \quad M(515) = -\dots,$$

$$M(516) = -\dots, \quad M(522) = -\dots, \dots,$$

$$M(555) = -\dots, \quad M(556) = -\dots, \quad M(566) = -\dots,$$

$$M(611) = \frac{1}{479001600} + \frac{\eta_1}{3628800} + \frac{\eta_1^2}{80640} + \frac{\eta_1^3}{4320} + \frac{\eta_1^4}{576} + \frac{\eta_1^5}{240} - \frac{31\eta_1^6}{720} - \frac{\eta_2}{40320} - \frac{\eta_1 \eta_2}{720} - \frac{\eta_1^2 \eta_2}{48} - \frac{\eta_1^3 \eta_2}{12} + \frac{5\eta_1^4 \eta_2}{8} + \frac{\eta_2^2}{48} + \frac{\eta_1 \eta_2^2}{4} - \frac{7\eta_1^2 \eta_2^2}{4} + \frac{\eta_2^3}{2} + \frac{\eta_3}{720} + \frac{\eta_1 \eta_3}{24} + \frac{\eta_1^2 \eta_3}{4} - \frac{7\eta_1^3 \eta_3}{6} - \frac{\eta_2 \eta_3}{2} + 3\eta_1 \eta_2 \eta_3 - \frac{\eta_3^2}{2} - \frac{\eta_4}{24} - \frac{\eta_1 \eta_4}{2} + \frac{3\eta_1^2 \eta_4}{2} - \eta_2 \eta_4 + \frac{\eta_5}{2} - \eta_1 \eta_5,$$

$$M(612) = \frac{4}{467775} + \dots, \quad M(613) = \frac{29297}{26611200}$$

$$+ \dots, \quad M(614) = \dots, \quad M(615) = \dots, \dots,$$

$$M(655) = \dots, \quad M(656) = \dots, \quad M(666) = \dots$$

Here in place of M_{ijk} we have used the notation $M(ijk)$. The three-dimensional matrix M_{ijk} is symmetric in the second

and third subscripts. Therefore we have only given the diagonal and subdiagonal elements in these indices. As in the case of the G and D matrices the structure of the polynomial elements of M varies only as a function of the first subscript. Therefore we have given complete expressions only for the elements $M(i11)$, and the other elements have been abbreviated where necessary.

We make two additional important comments and then proceed to the integration of the differential system (15), (16) and to the analysis of the properties of the trajectories.

In order to go over to a system with the lowest order of approximation it is necessary first to discard the highest equations with $i=N$ in the subsystems (15) and (16) and then in the other equations to set $A_N=0$ and $\eta_N=0$.

After integrating Eqs. (15) and (16) we find the Fourier amplitudes $\beta_1, \dots, \beta_{N+1}$ of the bounding surface [Eq. (3)] in terms of the coefficients $\eta_0, \eta_1, \dots, \eta_N$. To find them we must solve the linear system of equations

$$\eta_n = [(-1)^n / (2n)!] \sum_{m=1}^{N+1} m^{2n} \beta_m, \quad n=0, 1, \dots, N, \quad (17)$$

which is found by expanding the series (3) about $x=0$ in powers of x^2 . Note that if we express η_n in terms of β_n using Eq. (17), A_n in terms of α_n and η_0 using Eq. (8), and η_0 in terms of β_n using Eq. (17), then in place of Eqs. (15) and (16) for the unknowns η_n and A_n we find an equivalent system in the unknowns β_n and α_n .

3.2. The equations and their analysis for $N=1$

Consider Eqs. (15) and (16). For $N=1$ this system can be studied without difficulty. We use the autonomous property of Eqs. (15) and (16) and eliminate the time. Writing $W=A_1$ and $U=W^2$ and using the curvature K of the boundary at the extremal point $x=0$ as the variable, we find $K=1/R=2\eta_1$, where R is the radius of curvature. The function W is equal to the velocity of the boundary at the extremum, since the first of Eqs. (11) implies $\dot{\eta}_0=M_0$, and the moment is $M_0=\sum A_n$ [Eq. (10)]. For $N=1$ we have $\sum A_n=A_1$, since $\dot{\eta}_0=A_1$ holds. Hence it follows that $W=\dot{\eta}_0$. After these transformations Eqs. (15), (16) reduces to a single ordinary differential equation of the form

$$\frac{dU}{dK} = - \frac{2(U-gK)}{(1-K)(1-3K)}. \quad (18)$$

This equation enables us to find a complete qualitative description of the system (15), (16) in terms of the KU phase plane. We consider separately the cases $g=-1$, $g=0$, and $g=1$. Let us begin with gravitational waves.

3.2.1. The case $g=-1$, $N=1$. The structure of the phase plane is clear from Fig. 2a. It is more convenient to return to the variables W, K in place of U, K . The system has a singular point at the center ($W=K=0$). The center corresponds to hydrostatic equilibrium. This singular point is a focus. It develops as a result of the intersection of the isoclines $W=0$ (the K axis; see the figure, where $dW/dK=\infty$) and $K=-W^2$ (the parabola p , on which $dW/dK=0$ holds). The crests of the waves correspond to negative values of the curvature K , and the troughs to positive values. Equations (15) and (16)

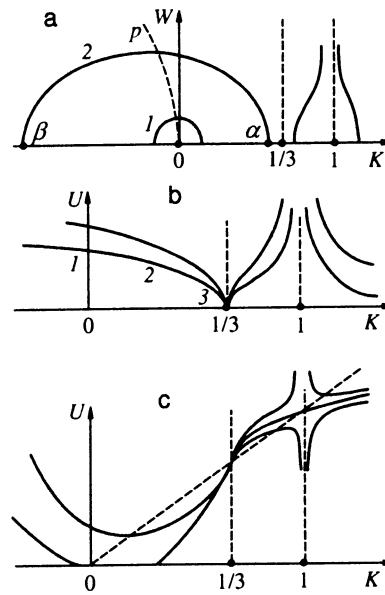


FIG. 2. a) Standing-wave oscillations. The physical picture is symmetric about the K axis, so only the upper half plane is shown. The trajectories 1 and 2 which are closed in the entire plane differ from the amplitude oscillations (see text). Frames a, b, and c are not drawn to the same scale. b) Linear (labeled by 1), transitional (2), and asymptotic (3) stages in the development of the Richtmyer–Meshkov instability in the $N=1$ model. In the limit $t \rightarrow \infty$ trajectories of the form 1–2–3 are attracted to the pencil of curves which enters the node 3. When this happens the curvature approaches $1/3$, the shape of the boundary stops changing, the velocity decays according to $W \propto 1/t$, and the displacement of the extremum grows logarithmically: $\eta_0 \propto \ln t$ [see Eq. (21)]. c) Rayleigh–Taylor instability. Of physical interest is the pencil of trajectories entering the node $U=K=1/3$, starting from the vicinity of the hydrostatic equilibrium point $U=K=0$. See also Fig. 12d.

describe the motion of gravitational standing waves. In a small neighborhood of the center the trajectories are close to circles, since here $|W| \approx |K| \ll 1$ holds and Eq. (18) in the variables W, K can be written approximately in the form $dW/dK = -K/W$. The crests and troughs of the standing waves are nearly symmetrical (trajectory 1 in Fig. 2a). The deviation from circular shape is a second-order effect in amplitude. At larger amplitudes the asymmetry of the trajectory becomes apparent. The crests and troughs are no longer symmetrical: now the crest amplitudes and their curvatures are larger than those of the troughs. Hence the circular trajectories are transformed into oblate closed curves shifted to the left of the center (trajectory 2 in Fig. 2a). These closed curves are bounded on the right by the isocline $K=1/3$, so in this approximation the curvature of a trough cannot be greater than $1/3$. At the points α and β in this figure, which is drawn for $W=0$, the motion goes to zero and the velocity changes sign.

3.2.2. The case $g=0$, $N=1$. This constitutes a dynamical model of the Richtmyer–Meshkov instability. The phase analysis of the system is given in Fig. 2b. In contrast to the case of gravitational waves here there are two singular points of different character. One of these is a node ($U=0, K=1/3$), while the other ($U=0, K=1$) is a saddle. They arise when the isoclines $K=1/3$ and $K=1$ on which $dU/dK=\infty$ holds intersect with the isocline $U=0$ on which $dU/dK=0$

holds. The phase diagram is symmetric with respect to inversion $U \rightarrow -U$. Since $U = W^2 > 0$ holds, in Fig. 2b only the upper half is shown.

Equation (18) for $g=0$ takes an especially simple form:

$$\frac{dU}{dK} = -\frac{2U}{(1-K)(1-3K)}.$$

The variables in it are separable and it can readily be integrated. The general integral takes the form

$$W = W_0 \sqrt{(1-3K)/(1-K)}, \quad W_0 = W(K=0). \quad (19)$$

Hence it follows that in the UK plane the motion can be described by a single trajectory. The other trajectories are found from it by a simple change of scale in U . Only trajectories of the form $1 \rightarrow 2 \rightarrow 3$ are physically meaningful (see Fig. 2b).

The time dependence is found from the original equations (15), (16), which in this case take the form

$$\dot{W} = -W^2/(1-K), \quad \dot{K} = W(1-3K). \quad (20)$$

Using the general integral (19) to eliminate the velocity W in the second of these equations, we find after integration the evolution of the curvature:

$$\frac{2}{3} \left(\sqrt{\frac{1-K}{1-3K}} - 1 \right) - \frac{2}{3\sqrt{3}} \ln \frac{\sqrt{3(1-K)} + \sqrt{1-3K}}{\sqrt{3} + 1} = W_0 t.$$

To be specific we have chosen the constant of integration here so that for $t=0$ the curvature vanishes.

Now we turn to the function $W(t)$. Expressing K in terms of W in the integral (19) and substituting the resulting expression in the first of Eqs. (20) we find after integrating over W

$$\frac{2}{3} \left(\frac{W_0}{W} - 1 \right) + \frac{1}{3\sqrt{3}} \ln \left(\frac{\sqrt{3} + 1}{\sqrt{3} - 1} \frac{\sqrt{3}W_0 - W}{\sqrt{3}W_0 + W} \right) = W_0 t.$$

Here the constant has been chosen so that $W(t=0) = W_0$ holds. From these expressions we find near the node, i.e., for $t \rightarrow \infty$, the following asymptotic expressions:

$$\eta_0 \rightarrow \left(\frac{2}{3} \right) \ln t, \quad W \rightarrow \frac{2}{3t}, \quad K \rightarrow \frac{1}{3} - \frac{8}{81W_0^2 t^2},$$

$$W \rightarrow W_0 \sqrt{\frac{9}{2} \left(\frac{1}{3} - K \right)}. \quad (21)$$

Note that the behavior of the trough $\eta_0(t)$ given by (21) inside the fluid is logarithmic (rather than algebraic with a small exponent).

In summary it should be pointed out that in Fig. 2b the physical trajectories have the form $1 \rightarrow 2 \rightarrow 3$. Small values of K correspond to the linear stage of the instability. Then a gradual approach to steady state occurs. The transition from the linear to the steady stage corresponds to the region 2 on this trajectory. Steady state, i.e., the node 3, is approached asymptotically in the limit $t \rightarrow \infty$. The shape of the trough and, in the case of several Fourier amplitudes in the potential, the ratios of these amplitudes also become time-independent. But the velocity and the amplitudes themselves continue to depend on time.

3.2.3. *The case $g=1, N=1$.* This is applicable to the Rayleigh–Taylor instability. Its phase diagram is shown in Fig. 2c. We analyze it briefly. There are three isoclines: the straight lines $U=K$ (the bisectrix) and the vertical lines $K=1/3$ and $K=1$. On the lines $U=K$ and $K=1/3$ the right-hand sides of Eqs. (15) and (16) vanish.³⁾ Consequently, their intersection point is a stationary point of this system. On the line $K=1$ the matrix G_{ij} becomes degenerate, going over to the subsystem (15). For $N=1$ this implies that the coefficient of \dot{A}_1 vanishes in this subsystem. Equation (18) for $g=1$ has two singular points $U=K=1/3$ and $U=K=1$ lying on the bisectrix. The first of these is a node and the second is a saddle point, with separatrices having slope dU/dK equal to ∞ and $1/2$. The asymptotic form of the pencil of trajectories entering the stationary point $U=K=1/3$ parallel to the vertical lines is

$$U - \frac{1}{3} = - \left(K - \frac{1}{3} \right) \ln \left(c \left| U - \frac{1}{3} \right| \right).$$

Here the parameter c runs through the incoming trajectories. The center $U=K=0$ is the hydrostatic equilibrium point: ($U=0$) describes the liquid at rest and ($K=0$) is the planar boundary. Points near the center represent deviations from equilibrium, where K is the deviation in the boundary and U corresponds to velocity perturbations.

Motion along a trajectory describing the displacement of the trough A (Fig. 1) toward the interior of the liquid is initiated in the vicinity of the center and goes from the center toward the node. It should be noted that on the portions of the trajectories above the bisectrix (see Fig. 2c) the velocity decreases, as occurs in the Richtmyer–Meshkov stability. This is an effect due to the next order beyond linear⁴⁾ and is absent from the linear theory of the Rayleigh–Taylor instability.

Only the half-plane $U > 0$ with real velocities W ($U = W^2$) is physically meaningful. At the point where a trajectory intersects the K axis the motion stops and turns around. According to the trajectories depicted in the KU plane in Fig. 2c, the motion can proceed in either direction, both from left to right and in the opposite direction. The points in the region $K < 0$ and those moving toward decreasing K describe the growth of the spikes T (Fig. 1).

Also, as described in Sec. 3.2.2, a trajectory consists of a linear part,⁵⁾ a transition, and an asymptotic part. It is a curious fact that the limiting curvature in the trough at the point A (Fig. 1) attained in the limit $t \rightarrow \infty$ is the same in the cases of the Rayleigh–Taylor and Richtmyer–Meshkov instabilities.

Note that treatments of the Rayleigh–Taylor instability frequently concern themselves with the model $g=1, N=1$ described above. The reasons for this are, first, it is simple, and secondly, it gives a good description of the results of crude⁶⁾ numerical calculations. This is called the Layzer model or solution.^{25,26} This model has been improved upon somewhat here. The improvement consists of making it simpler and more transparent. This has the side effect of permitting it to be augmented by a detailed general analysis. This is possible because by making substitutions we have reduced the problem to the simple⁷⁾ equation (18), thereby permitting

the analysis to be carried out in terms of the phase plane. This analysis is what leads to the conclusions regarding the general structure of the solutions.

But we have not studied the case $g=0$. By virtue of the homogeneity of the subsystem (15) in amplitude for $g=0$, this case is found to admit complete integration. This a new result. It is interesting that the qualitative behavior of the models in Secs. 3.2.2 and 3.2.3 is similar; in particular, for $g=0$ there can also be a time-independent asymptotic state.

Now we turn to cases with $N>1$. We start with the simplest of these, connected with $N=2$ and the homogeneous ($g=0$) subsystem (15).

3.3. Richtmyer–Meshkov case for $N=2$

As we proceed to the analysis of the situation that arises in higher orders of approximation, it should be noted that (as will become apparent below) there is a qualitative difference between the behavior of the system for $N=1$ and for $N>1$. This difference consists in the following. While a solution of Eqs. (15), (16) exists for $N=1$ for all t from 0 to ∞ (see Secs. 3.2.2 and 3.2.3), for $N>1$ matters are different. It is found that for $g=0$ and $g=1$ all trajectories of physical interest beginning from an arbitrary neighborhood of the hydrostatic equilibrium point display singular behavior. What happens is that at some finite time t_c on the boundary a singularity develops at the minimum of the trough. If we follow the trajectories of the system (15), (16), then we can

see that at this time the plot of a point moving along the trajectory is blocked by a hypersurface S_G on which the matrix of the coefficients G_{ij} given by (15) becomes degenerate. The formation of the singularity is inevitable because the trajectories and the hypersurface are so constructed that the latter attracts the trajectories.

The simplest system that displays singular behavior is obtained for $g=0, N=2$. Because the system is autonomous and homogeneous in the amplitudes A , as follows from the condition $g=0$, it can be reduced to a system with a three-dimensional phase space. Let us again write $K=2\eta_1$. In order to make use of the homogeneity we introduce the amplitude ratio $\rho=A_2/A_1$ in place of one of the amplitudes. Specifically, we write $A_2=A_1\rho$ in Eqs. (15), (16). After this we find

$$\begin{aligned} \dot{A}_1 &= A_1^2(G_{22}M_1 - G_{12}M_2)/|G|, & \dot{\rho} &= A_1 Q/|G|, \\ \dot{\eta}_i &= A_1(D_{i1} + D_{i2}\rho), \\ M_i &= M_{i11} + 2M_{i12}\rho + M_{i22}\rho^2, & Q &= -G_{21}M_1 \\ & & & + G_{11}M_2 - G_{22}M_1\rho + G_{12}M_2\rho, \end{aligned} \quad (22)$$

where $i=1,2$ and $|G|$ is the determinant of the matrix G . It is already clear that the equation for A_1 separates from the rest of the system. Substituting the expressions (22) for G , M , and D from Sec. 3.1 and using the differential dK in place of dt , we find

$$\begin{aligned} \frac{d\rho}{dK} &= -(-K + 3K^3 + 6\rho - 17K\rho + 6K^2\rho + 15K^3\rho + 12\rho^2 - 32K\rho^2 + 12K^2\rho^2 + 24K^3\rho^2 - 16K\rho^3 + 12K^3\rho^3 + 24\eta_2 \\ &+ 120\rho\eta_2 + 192\rho^2\eta_2 + 96\rho^3\eta_2)(6 - 37K + 75K^2 - 57K^3 + 9K^4 + 24\rho - 112K\rho + 186K^2\rho - 120K^3\rho + 18K^4\rho \\ &+ 24\eta_2 - 72K\eta_2 + 96\rho\eta_2 - 144K\rho\eta_2)^{-1}, \\ \frac{d\eta_2}{dK} &= \frac{-1 + 10K - 15K^2 - 16\rho + 80K\rho - 60K^2\rho + 120\eta_2 + 240\rho\eta_2}{24(-1 + 3K - 4\rho + 6K\rho)}. \end{aligned} \quad (23)$$

Consider the ρ, η_2, K space of Eqs. (22) or the equivalent system (23). They are two geometrical (i.e., connected with the shape of the boundary) variables η_2 and K , and one variable ρ that results from the Fourier amplitudes of the potential expansion. At the stationary points of Eqs. (15), (16) with $g=0$ and an arbitrary value N the amplitudes A_i are equal to A_i^{stat}/t , where the A_i^{stat} are constants. The amplitude ratios A_i/A_j and the geometrical variables η_i (except for η_0) are also constant. For η_0 we have

$$\eta_0 = -(\ln t) \sum_{i=1}^N A_i^{\text{stat}}.$$

For Eqs. (22) or (23) the constancy of these variables requires $Q = \eta_{i1} + \eta_{i2}\rho = 0, i=1,2$. After performing linear

operations to eliminate ρ and η_2 from this algebraic system we find an equation determining the unknown K at the stationary point. It is equal to

$$285K^4 - 555K^3 + 461K^2 - 177K + 26 = 0,$$

and has no real roots. Consequently, the system (22) or (23) has no stationary points. The right-hand sides of Eqs. (22), except for $|G|=0$, contain polynomial expressions and have no singularities in the finite region. The singular behavior of the solutions (22) can therefore be attributed only to the vanishing of $|G|$.

Let us turn to the investigation of the surface S_G in which $|G|=0$ holds. The elements of the matrix G_{ij} depend only on the geometrical variables, so the surface S_G is parallel to the ρ axis (see Fig. 3a). This forms a “partition” in ρ, η_2, K space, separating it into two parts. Hence it follows that it is convenient to treat projections on the K, η_2 and $K,$

ρ planes (see Figs. 3b and c). Another important fact is the following. We will study the evolution of the system in the case when the initial perturbation is given by the first harmonic alone. In this case only the initial values of the variables A_1 and (or) β_1 are nonzero [see Eqs. (3), (4), and (8)]. The important thing here is that since A_1 drops out of Eqs. (22) and we have $A_2(t=0)=0$, it suffices to treat trajectories that start only on a line lying in the $K \eta_2$ plane (i.e., in the plane $\rho=0$ or $A_2=0$) given parametrically by the relations $K=\beta_1$, $\eta_2=\beta_1/24$, which follow from the power-series expansion of $\cos x$ about zero; see Fig. 3b. This permits us to narrow the class of initial points.

The results of integrating Eqs. (23) are shown in Figs. 3b and 3c. As can be seen, for a broad class of initial data the dynamical system approaches the surface S_G .

Now let us extend the analysis of Eqs. (15), (16), to other values of N . To conclude the description of the case $g=0$, $N=2$ we note that it was treated in a separate subsection only to make clearer the attractive properties of the surface S_G with respect to a pencil of trajectories embracing a broad region of initial data. To obtain persuasive evidence in favor of the assertion that the singularity touches the bounding surface and about the behavior of the higher approximations and especially their convergence is much more important, of course.

3.4. Integration of the higher multimode approximations

The equations (15), (16) derived analytically above have been integrated for all cases in the range $1 \leq N \leq 6$. The values $g=0, \pm 1$ have all been investigated. A wide class of combinations of values of the first amplitudes A_1 and β_1 were chosen as initial conditions [see Eqs. (3), (4), and (8)], to which were added higher harmonics with amplitudes small in comparison with the first.

We briefly characterize the integration scheme. The Runge-Kutta method was used. In calculations of Eqs. (15), (16) the first subsystem (15) of these equations was written in the form $G_{ij} \dot{A}_j = (\text{r.h.s.})$. At each integration step it was treated as a system of linear equations for the unknowns \dot{A}_j .

We will now present the results of the integration. To avoid repetition we restrict ourselves here mainly to a verbal description, since the corresponding plots will be needed below in discussing the convergence of the approximations and in comparing these results, which we will call analytical, with the first numerical simulation. And so the calculations reveal that the trajectories closely approach the surface S_G . The absolute value of $|G|$ decreases by two or three orders of magnitude. The functions $|G|/|G_0|$ of t are shown in Fig. 4; here $|G_0|$ gives the value of the determinant at the initial time. The function $|G|$ at $N=6$ is not shown, since in consequence of the enormous complexity of this expression problems arise with memory in the FORTRAN compilation. The smallness of the distances to which the trajectories approach S_G is determined by the numerical sources of error due to truncation and roundoff. This was the case for all values of N except⁸⁾ $N=1$ and, as already noted, over a broad class of initial data.

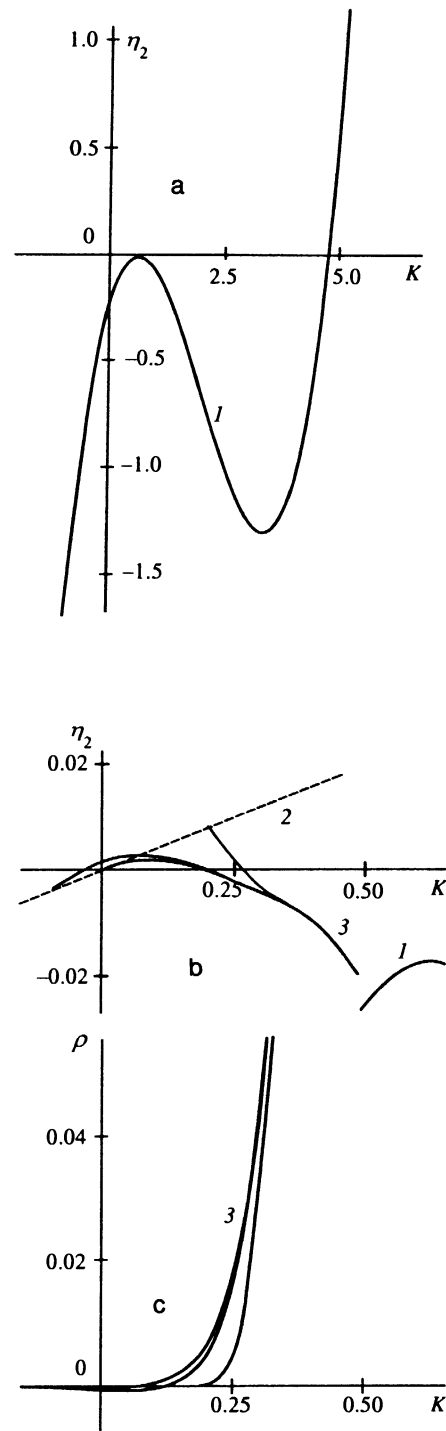


FIG. 3. Shape of the surface S_G and trajectories in the case $g=0$, $N=2$. This case is noteworthy because its small spatial size allows the surface S_G to be depicted and because it shows how the trajectories approach S_G . a) Projection of the surface S_G on the $K \eta_2$ plane. This projection is a curve on the latter plane, since S_G is parallel to the ρ axis. The curve is labeled with I . The motion of interest to us occurs in the subregion of this plot located between the zero and the maximum of trace I (see Fig. 3b). b) Projections of the trajectories on the $K \eta_2$ plane (a family of curves 3). The trajectories approach the surface S_G (trace I). The initial points are on the line $\eta_2=K/24$ (the broken trace labeled 2). In the text it is explained why they are on this line. c) Projections of the trajectories on the $K \rho$ plane (the family of curves labeled 3). The trajectories start at the $\rho=0$ plane (the $K \eta_2$ plane), which in this projection appears as the K axis. For this example we use the same trajectories as in Fig. 3b. The sharp increase in ρ is due to the approach of the singularity to the boundary. It occurs at the same time as the approach to the surface S_G .

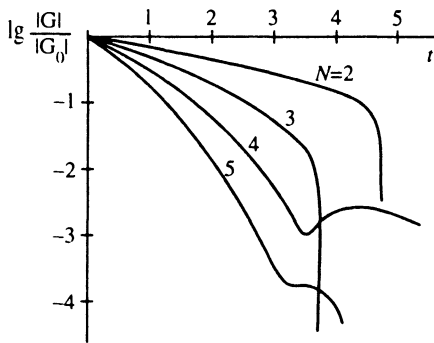


FIG. 4. Approach to the hypersurface S_G as $|G| \rightarrow 0$. The numbers indicate the value of N .

4. TRAJECTORY APPROXIMATIONS AND THEIR CONVERGENCE AS A FUNCTION OF N

From the above it follows that in all cases⁹⁾ the trajectories of Eqs. (15), (16) have a terminal point in time, associated with the surface S_G . It might be asked, what relation does this have to the continuum system (1), (2)? To be sure, a conclusion reached by means of a *single* finite-order approximation must be regarded as hypothetical, even if the approximation is of high order. It becomes rigorous only in connection with an investigation of convergence. Let us now treat this important question.

The analytical solution of Eqs. (1), (2) was obtained by expanding the dependent variables in a complete orthogonal basis. The exact solution was approximated by means of a Galerkin truncation of this expansion. Let

$$\begin{aligned} \mathbf{k}^N(t) &= \{k_1^N, k_2^N, \dots, k_N^N, k_{N+1}^N, \dots, k_{2N}^N\} \\ &= \{\eta_1^N, \eta_2^N, \dots, \eta_N^N, A_1^N, \dots, A_N^N\} \end{aligned}$$

be the coefficients of this truncation. Here the superscript N indicates the adjustable order of the approximation.

The boundary-value problem (1), (2) was approximated using the difference system $d/dt(\mathbf{k}^N) = \mathbf{f}^N(\mathbf{k}^N)$. The calculations were performed up to high values of N ($N=6$; see Sec. 3). A great deal of attention was devoted to the question of convergence. The dependence of the deviations

$$\begin{aligned} \Delta^N(t) &= \|\mathbf{k}^N(t) - \mathbf{k}^{N-1}(t)\| \\ &= \sum_{n=1}^{N-1} (|\eta_n^N - \eta_n^{N-1}| + |A_n^N - A_n^{N-1}|) \end{aligned} \quad (24)$$

as a function of N was carefully analyzed. The functions $k_i^N(t)$ and the partial deviations

$$\begin{aligned} \Delta k_i^N(t) &= |k_i^N - k_i^{N-1}|, \quad \Delta A_i^N(t) = |A_i^N \\ &\quad - A_i^{N-1}|, \quad \Delta \eta_i^N(t) = |\eta_i^N - \eta_i^{N-1}| \end{aligned}$$

are shown¹⁰⁾ in Figs. 5–8. As can be seen, the trajectory approximations converge exponentially even when the iteration step q of the corresponding geometrical progression ($\Delta^{N+1} = q\Delta^N$) is large. This step is shown in the form of a vertical segment of length $q \approx 4.7$ in Fig. 5b. The sharp downward-pointing peaks in the lower figures 5b, 6b, 7b, and 8b result from the intersection of the functions shown in the upper figures 5a, 6a, 7a, and 8a; the lower figures display the functions $\log |k_i^N(t) - k_i^{N-1}(t)|$, which go to $-\infty$ for $k_i^N = k_i^{N-1}$. The typical examples shown in Figs. 4–8 were calculated for the case $g=1$. Initially the boundary was planar. The initial velocity field was given by a single harmonic with amplitude $A_1(0) = 0.112$. Convergence is observed over the entire range of t on which a continuous solution is found.

The divergence of the trajectories approaching S_G (see, e.g., Fig. 8a) and the decrease in $|G|$ enable us to estimate the time t_c . In particular, for the examples shown in Figs. 4–8 we find $t_c = 3 \pm 0.5$.

5. WHAT THE FAILURE OF THE APPROXIMATION MEANS

In Secs. 3 and 4 it has been shown that there exists a time t_c at which the trajectory terminates. In the limit $t \rightarrow t_c$ the system (15), (16) ceases to give a good approximation to the conditions (1), (2). In order to understand what this observation implies we should pause briefly to consider the technique employed.

It turns out that it has a direct relation to the widely used collocation technique. In this technique collocation points $\{x_i\}$ are distributed on the symmetric half of a period. Let $x_0 = 0 < x_1 < \dots < x_N$ (see Fig. 9a). The shape of the boundary is given by the set of values $\eta_0, \Delta_1, \dots, \Delta_N$, where $\eta_0 = \eta(x_0, t)$ and $\Delta_i = \eta_i - \eta_0$, $\eta_i = \eta(x_i, t)$. We expand the potential in a series $\varphi = \sum_{n=1}^N A_n \cos nx \exp(n\Delta)/n$, where $\Delta = y - \eta_0$. Then the equations that follow from the conditions (1), (2) take the form

$$\dot{\eta}_0 = -\sum A_n, \quad \dot{\Delta}_i = \sum_{n=1}^N A_n - \sum_{n=1}^N A_n C_{ni} e^{n\Delta_i}$$

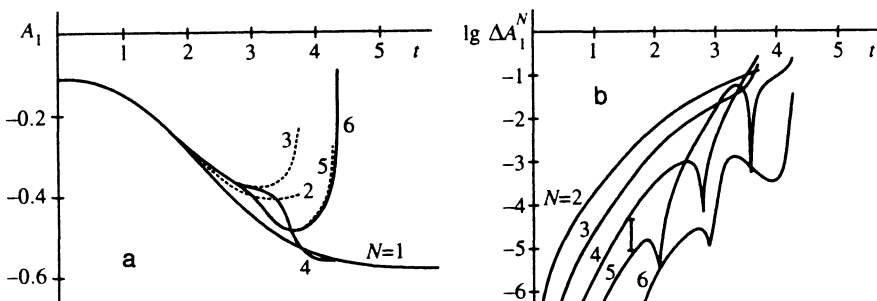


FIG. 5. a) The function $A_1(t)$ is shown. The values of N are given by the labels on the curves. The trajectories begin to steepen as they approach S_G . The initial data are given in the text; here $g=1$. b) Exponential convergence of the approximations as a function of N . The labels give N in accordance with the definition (24).

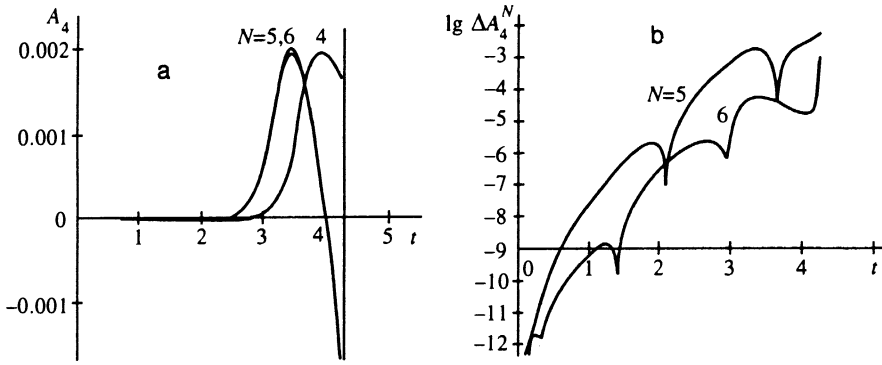


FIG. 6. a) The variation of $A_4(t)$. b) The variation of $\log \Delta A_4^N(t)$. Here the numbers indicate the value of N .

$$-\sum_{m=1}^{N+1} \sum_{n=1}^N mA_n b_m S_{mi} S_{ni} e^{n\Delta_i}, \quad (25)$$

$$\begin{aligned} & \sum C_{ni} e^{n\Delta_i} \dot{A}_n / n \\ &= \sum A_n A_m C_{ni} e^{n\Delta_i} - \frac{1}{2} \left[\left(\sum A_n C_{ni} e^{n\Delta_i} \right)^2 \right. \\ & \quad \left. + \left(\sum A_n S_{ni} e^{n\Delta_i} \right)^2 \right] - g(\eta_0 + \Delta_i) + c(t), \quad (26) \end{aligned}$$

where $C_{ni} = \cos nx_i$, $S_{ni} = \sin nx_i$, $\Delta_0 = 0$. Function η_0 and function $c(t)$ connected with calibration in the Eq. system (26) are dismissed by subtracting the equation with $i=0$ from the equations with $i \neq 0$. The coefficients b_m are found from the linear equations $\eta_j = \sum b_m C_{mj}$.

Since the line L ($y = y_{\text{down}}$), which limits the singularities (5), is far from the collocation points a, b, \dots (Fig. 9a), the method works and the approximations converge. As the perturbations grow the line L approaches the fluid (cf. Fig. 9a and 9b). But if one collocation point lies beyond this line (Fig. 9b), then we cannot use a Fourier expansion to calculate the φ that appears in it. Consequently, Eqs. (25), (26) no longer approximate the conditions (1), (2).

Each set $\{x_i\}$ corresponds to its own system (25), (26). Consider systems obtained in the limit in which the collocation points approach a limit, $x_i \rightarrow x_{ac}$. As the distance between the points x_i decreases, for calculations with a fixed number of bits in the mantissa the accuracy decreases. In order to avoid this, we consider linear combinations of the collocation equations:

$$a_1 = \frac{u_1 - u_0}{x_1 - x_0} = 0, \quad a_2 = \frac{u_2 - u_1}{x_2 - x_1} - \frac{u_1 - u_0}{x_1 - x_0} = 0, \quad \dots$$

These are differences of successively increasing order. In place of the system $u_1 = 0, u_2 = 0, \dots$ we arrive at the system $a_1 = 0, a_2 = 0, \dots$. It is quite obvious that the latter corresponds to algebraic approximations of the conditions (1), (2). We approach it asymptotically as the points x_i converge. It is therefore natural to call the method based on Eqs. (15), (16) the method of asymptotic collocations. In order to emphasize the difference between these two methods we will call the method based on Eqs. (25), (26) ordinary collocations.

Consider the problem of detecting the approach of a singularity to η using the method of asymptotic collocations. It is evident that if the point x_{ac} is located somewhere outside the point A , e.g., on the crest T or at the point B (Fig. 9c), then detection will be impossible. In fact, the failure of the approximation using the equations (15), (16) associated with this location of x_{ac} would still not suffice to prove that contact had taken place. The trouble is, there will be no way to ascertain whether the singularity moves along trajectory 1 or trajectory 2 (Fig. 9c). The only exception occurs when the point x_{ac} lies in the trough A . In this case the failure of the approximation implies that the singularity has reached η at the point A (see below).

6. BEHAVIOR CLOSE TO CRITICALITY

Assume $x_{ac} = 0$. In the limit $t \rightarrow t_c$ the trajectories approach S_G , $\dot{A}_n \rightarrow \infty$, and the series (4) and (8) diverge. Since these series converge for $y < y_{\text{down}}$, then, as noted above, this implies that the lower singularity closely approaches η . It approaches η at the minimum of the trough (see Fig. 9c), i.e., at the point A .

In fact, if the singularities slowed down in the course of time and stopped at locations fixed with respect to η and at finite distances from η , then the integration of Eqs. (15), (16)

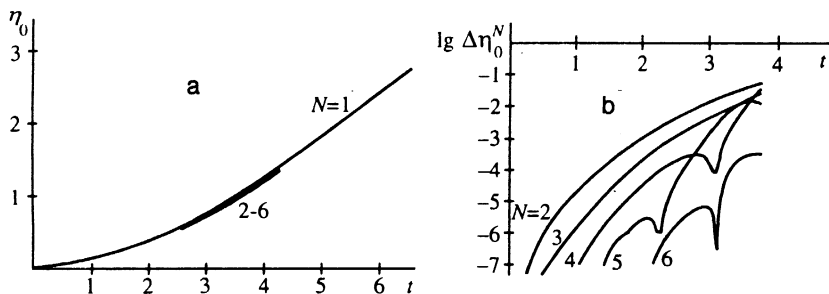


FIG. 7. a) The variation of $\eta_0(t)$. b) The variation of $\log \Delta \eta_0^N(t)$. Here the numbers indicate the value of N .

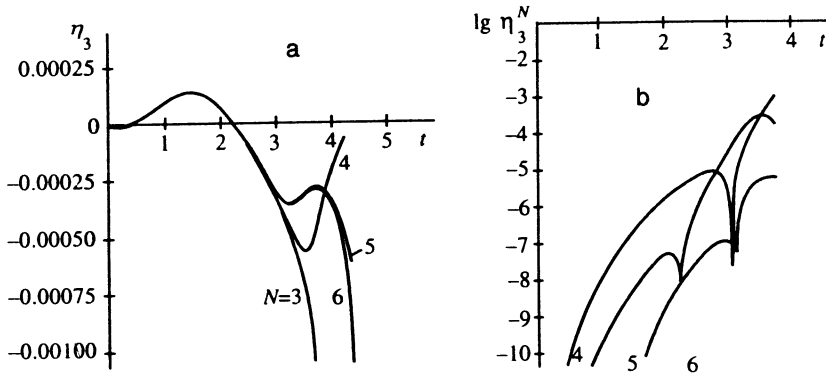


FIG. 8. a) The variation of $\eta_3(t)$. b) The variation of $\log \Delta \eta_3^N(t)$. Here the numbers indicate the value of N .

with respect to time would last an infinitely long time for all N . This follows from the fact that, as is well known,²⁷ the time-independent form of Eqs. (15), (16), which is found from these equations for $\dot{A}_n=0$ and $\dot{\eta}_n=0$, describes a solution which is continuous and stationary everywhere. In the limit $t \rightarrow \infty$ this solution would be approached.

The approximation of Eqs. (15), (16) would still hold even if the singularity approached η somewhere on the lateral surface at a higher distance from the point A. This possibility is illustrated in Fig. 9c, trajectory 1.

Consider the sub- and supercritical space-time vicinity of the point and the time of approach. In order to deal with what happens, let us analyze the following problem.

For $t=0$ let a wedge-shaped indentation with a rounded vertex be made in the fluid (Fig. 10a,a'). Assume that the pressure in the indentation satisfies $p_0=\infty$, while the pressure at infinity is $p_\infty=0$. Hence ∇p in the vicinity of the rounded point is a finite quantity. Let the initial velocities be equal to zero.

It is not hard to see that the separation between isobars become smaller near the vertex of the indentation, so that ∇p and the associated acceleration of the fluid is largest at the vertex. Consequently, the wedge can become sharper spontaneously (see Figs. 10b and 10b'). If so, then there exists a time t_c such that the curvature at the vertex diverges. For $t > t_c$ η becomes discontinuous and forms a new piece of surface η consisting of Lagrangian particles located at the vertex point at time t_c (Fig. 10c).

For the concave case the motion of the fluid is accompanied by elongation of its boundary η . From the above comments it follows that this elongation is not continuous everywhere. A discontinuity of the boundary implies that if we color η then after some finite time an uncolored portion of finite extent develops on η . This portion consists of a segment separated by the two points A and B (Fig. 10c) from the colored part of η . If a and b are points (Fig. 10b and 10c) located on opposite sides of the collapse point on η , then with continuous elongation we have $|\delta \mathbf{r}_{ab}(t)| = f(t) |\delta \mathbf{r}_{ab}(0)|$, where we have written $\delta \mathbf{r}_{ab} = \mathbf{r}_a - \mathbf{r}_b$ and $f(t)$ is a function which increases, possibly exponentially. When discontinuity develops this relation breaks down, since when $\delta \mathbf{r}_{ab}(0)$ contracts to zero it is not necessary that the segment $\delta \mathbf{r}_{ab}(t)$ also contract to zero for $t > t_c$ (see Figs. 10b and 10c).

Even after discontinuity develops the vertex of the in-

dentation remains in the region of enhanced values of ∇p . Hence the motion of its neighborhood should outstrip the other parts toward the interior of the fluid. Consequently, in the region of the vertex a leader forms, which points into the fluid in the direction of the densest isobars.

It is evident that in our case the trough is in some sense equivalent to an indentation in the fluid. Specifically, in the case of a trough the curvature is also largest at the point of minimum depth. Consequently, this problem is likely to be related to our case.

For additional confirmation of the above account and to study the neighborhoods of the points on the new surface which are adjacent to A and B of the old (Fig. 10c), we turn to two-dimensional hydro- and gasdynamic codes.

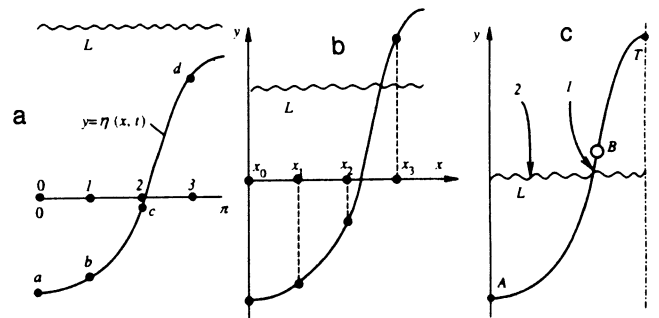


FIG. 9. The approach of the singularities and the failure of the approximation. Here the coordinates of the collocation points are indicated by y . The singularities are above the line L , indicated by the wavy line. The potential expansion converges in the half-plane below L for $y < y_{\text{down}}$. Conventional (a,b) and asymptotic (c) collocations are shown on the symmetric half-period $[0, \pi]$. The shape of the boundary at t_1 (a) and for $t_2 > t_1$ (b) is given. b) Elongation of the liquid spike as a function of time and approach of the singularities and therefore of the line L to the liquid. The situation is shown in which one of the collocation points (the point x_3) is beyond the line L . Consequently, the point x_3 is found in the half-plane in which the Fourier expansions (4) and (8) for the potential diverge, so that the values of the potential and velocity cannot be calculated by means of these expansions. c) Locations of the point x_{ac} at which the power-series expansion is carried out in the asymptotic collocation technique, in connection with the problem of detecting the approach of a singularity to η . If $x_{ac} \neq 0$ holds, e.g., let B be a collocation point. The fact that Eqs. (15) and (16) no longer approximate (1), (2) still does not imply that the singularity has reached η . Specifically, it can move tangent to η as shown in trace 1 or past it as shown in trace 2. Traces 1 and 2 depict the lowest singularity.

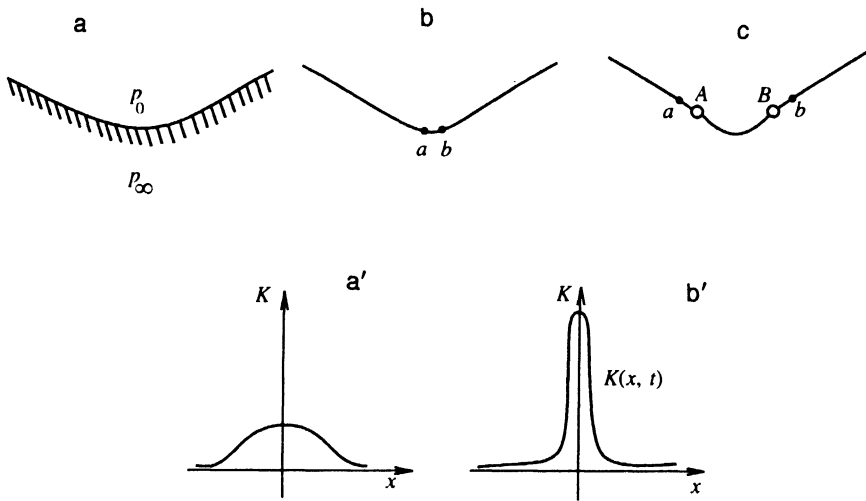


FIG. 10. Initial shape (a) and curvature $K(x, t=0)$ (a') of the boundary. The fluid is indicated by hatching. b, b') Illustration of the hypothesis that the sharpness of the spike increases with time. At time t_c a sharp wedge develops. c) At $t=t_c+0$ the point of the wedge breaks up and a new surface forms between the points A and B.

7. NUMERICAL SIMULATION

We begin with the properties of the Eulerian codes used. In order to make the results more reliable we checked them by using two different algorithms. One of these is well known. It is based on the particle-in-cell (PIC) method,²⁸ which is widely used in gasdynamics. At low Mach numbers this algorithm approximately describes the dynamics of an incompressible liquid. The code was written by A. Yu. Dem'yanov. The other algorithm applies directly to the incompressible case and is related to the artificial-viscosity method, generalized by A. V. Chekhlov to an inhomogeneous fluid.²⁹ The results obtained using these two codes agree. A series of calculations was carried out in which we varied the initial conditions over a wide range. This includes the sign

and magnitude of g , the density ratio μ of the liquids at the interface, the grid spacing, the Courant number which limited the time step, and the boundary conditions at the upper and lower limits of the domain of the calculation. Any detailed discussion of the numerical treatment would go far beyond the scope of the present work. Here we present only a summary of the main results.

The typical evolution of η is shown in Fig. 11. In this case we took $\mu=1/10$, $\mu=\rho_l/\rho_h$, and the calculation was performed using the artificial-viscosity technique with $A_1(0)=0.11$, $A_n(0)=0$, $n>1$, $\eta_m(0)=0$, $m\geq 0$, and $g=+1$. These initial data correspond to the case whose analytical solution is shown in Figs. 4–8. Here and in what follows ρ_h and ρ_l represent the density of the lower (heavy) and

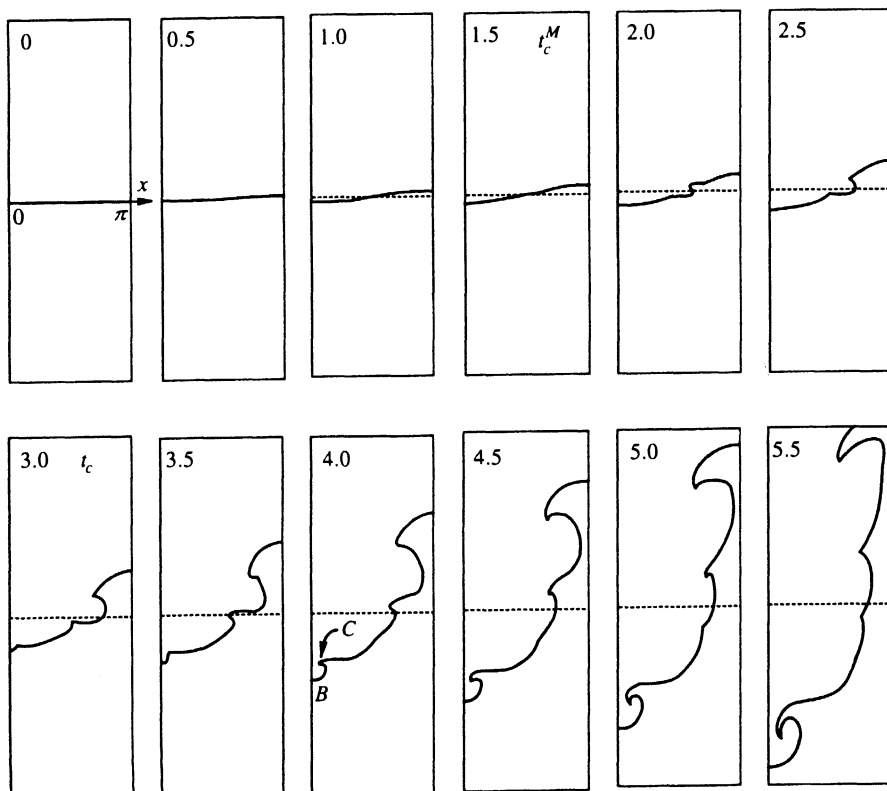


FIG. 11. Evolution of η , collapse, and formation of a discontinuity as found in numerical simulation. The values of the parameter are given in Sec. 7. The time is shown in the upper left corner. Collapse occurs at time $t_c \approx 3$ at the bottom of the trough. For $t>t_c$ there is a bubble B and spike C (marked with an arrow). The figure shows the symmetric half of a period. Half of the bubble B and of one of the two symmetric spikes are missing.

upper (light) fluids, respectively. The mesh spacing in x and y in this case was $\delta_x = \delta_y = \lambda/110$. The displaced density contours are shown on which the density is equal to the average intermediate value $(\rho_h + \rho_l)/2$.

The principal content of the present work is related to the study of hydrodynamic collapse. The continuous evolution of the system has been followed analytically up to the time of collapse at the minimum of a trough. Here we compare the analytical calculations with the results of the numerical simulation for $t < t_c$ and compare the values of t_c obtained analytically and numerically. Because of space limitations we can devote less attention to questions here regarding the form of the solution after the time t_c and about the effect on the solution of finite values of the parameter μ .

Let us analyze Fig. 11. Two noteworthy occurrences are revealed here. The first takes place at time $t_c^M \approx 1.5$, while the second is at time $t_c \approx 3$. The event that occurs at $t = t_c$ is similar to the collapse studied analytically above. Evidence for this comes from the agreement between the analytical and numerical solutions for $t < t_c$ and the agreement in the localization of the collapse and the values of the time t_c . The point x_c at which collapse is localized is equal to zero. We see that at t_c the surface η breaks up and a bubble is initialized on it between the point C and the minimum of the trough. A spike C develops at the point where the new surface makes contact with the old one. Thereafter the area of the new surface grows, since the spike moves away from the minimum point.

It can be shown that what happens at $t = t_c^M$ at the point $x_c^M \approx \pi/2$ is related to the fact that $\mu \neq 0$. The codes used here do not allow the case $\mu = 0$ to be simulated. To minimize the influence of μ we therefore chose the smallest possible values of this parameter. It is well known that for $\mu \neq 0$ mushroom shapes develop. The event that occurs at t_c^M is probably related to the onset of this process. This question must be discussed in a separate publication. Here we will only point out some isolated details.

A detailed comparison between theory and simulation was performed. In the forms of the codes used the evolution of the Fourier components of the potential, which is intended for the future, was not implemented. We therefore restrict ourselves here to transforming $\eta(x, t)$. Figure 12a shows a comparison between the theoretical and numerical shapes at time t of this quantity for $t_c^M < t < t_c$. At times $t < t_c^M$ these shapes are essentially identical over the whole range of values $x \in (0, \pi)$. For $t > t_c^M$ they remain very close to one another in the subinterval $x \in (0, x_c^M)$. But in the neighborhood of the tip T of the spike the aerodynamic drag due to the low-density fluid begins to have an important effect on the motion of this spike. This is because the parameter μ is nonzero. As a result, the shapes $\eta(x, t)$ begin to differ for $x \in (x_c^M, \pi)$.

The situation is similar for the other initial data as well. As a result, the theoretical and numerical shapes of η before collapse ($t < t_c$) agree with one another. Rather naturally, this also implies that the theoretical and numerical values of t_c agree. Because of its importance we discuss the information obtained regarding this point in more detail. The corresponding plots are shown in Figs. 12b, c, and d. They display the

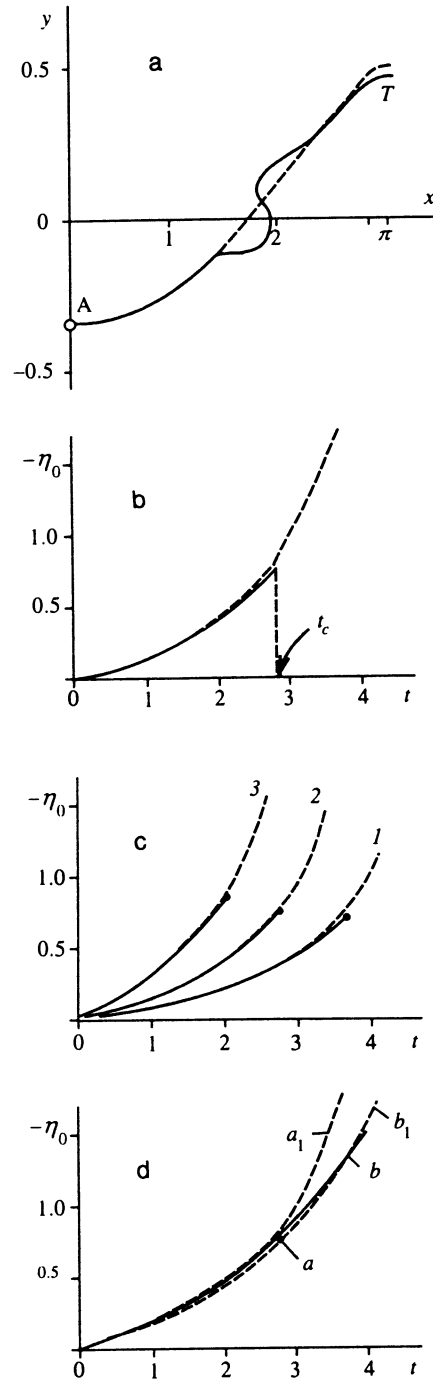


FIG. 12. a) Comparison of the theoretical (broken trace, $N=6$) and numerical (solid trace) forms of $\eta(x, t)$ at time $t=2$. The values of the parameters are as in Fig. 11. b) Termination of the theoretical curve and kink on the function $-\eta_0(t)$ obtained numerically. The values of the parameters are as in Fig. 11. In figures b), c), and d) the solid traces are found theoretically and the broken ones from the simulation. c) Comparison of the times t_c on the numerical and theoretical curves. The initial data associated with the pairs of curves 1, 2, and 3 are given in the text. d) Theoretical curves for $N > 1$ (curve a, calculated for $N=6$) and for $N=1$ (curve b). Curve b continues to $t = \infty$; see Fig. 2c. For $t < t_c$ trajectories with different values of N are essentially identical. We also give curves found numerically for appropriate (curve a_1) and coarse (curve b_1) grids. As can be seen, the times t_c agree on curves a and a_1 . In addition, curves b and b_1 agree.

time variation $\eta_0(t)$ of the displacement of the minimum of the trough. The plots in b and c and trace 2 in Fig. 12c refer to the initial data for $A_1(0) = 0.11$, presented above. Traces

1 and 3 in Fig. 12c were obtained for $A_1(0)=0.055$ and $A_1(0)=0.22$, respectively. The solid traces indicate the theoretical dependence obtained for $N=6$ (see also Fig. 7a). The broken traces indicate the results of the theoretical simulation. For $N>1$ all the theoretical curves terminate at time t_c , indicated by the arrow in Fig. 12b. At approximately the same time on the surface η a bubble and spike form (see Fig. 11). The plot of $-\eta_0(t)$ obtained from the numerical simulation shows that this is accompanied by an enhanced rate of increase of the quantity $-\eta_0$ (Figs. 12b, c, and d). The times at which the theoretical curves terminate agree satisfactorily with the formation times of the spike and bubble for various initial conditions (Fig. 12c).

The theoretical trajectories for $N=1$ do not have termination points (cf. Fig. 12d, trace *b*). For $0<t<t_c$ the trajectories referring to different values of N (including $N=1$) are essentially identical. In any case, on the scale shown in Fig. 12d the difference between the curves is not discernible.

The results of the numerical simulation depend on the grid spacing used (Fig. 12d, traces a_1 and b_1). This variation is as follows. Let N_x be the number of cells in a square lattice per wave period. There exists a minimum value $(N_x)_{\text{thr}}$ which separates the grid resolution which is unsuitable to describe the discontinuity and that in which the grid is sufficiently fine to describe it. For $N_x>(N_x)_{\text{thr}}$ the dependence on N_x drops out. The value of N_x was varied over a wide range from 20 to 200. It was found that the magnitude of the threshold is given by $(N_x)_{\text{thr}}\sim 50$, depending on the numerical scheme used.

The comparison between theory and simulation shows that the results on coarse grids agree with the theoretical case $N=1$ (cf. traces *b* and b_1 in Fig. 12d). But the results obtained with grids appropriate for describing the discontinuity agree with the multimode theory (cf. traces *a* and a_1 in Fig. 12d).

8. IS THE PROBLEM WELL-POSED?

In the foregoing treatment we have considered the problem of a free surface in the case when the amplitudes A_n and η_n of the harmonics in the series (8) and (3) drop off exponentially at $t=0$ [cf. Eq. (5)]. We ask whether the small-scale modes with $n\gg 1$ can effect the evolution of modes with $n\sim 1$. Let us treat the time evolution using the WKB approximation, which gives an upper limit to the amplitudes of the small-scale modes. As a result we obtain the estimate

$$A_n(t)\sim c_1(n)\exp\left[-(\ln c)n + \sqrt{\frac{1-\mu}{1+\mu}} n t\right].$$

The definitions of c and c_1 are given in Eq. (5). Here we have used an expression for the Rayleigh–Taylor growth rate $\gamma = \sqrt{gk(1-\mu)/(1+\mu)}$ in units such that $g=k=1$. From this estimate it follows that $A_n(t_*)\sim 1$ occurs at time $t_*(n) \sim \sqrt{n}$. Thus, we arrive at the conclusion that the evolution of the long-wavelength modes can be studied in this manner.

9. CONCLUSION

In this work we have studied the evolution of the free surface of a liquid. To be specific we have treated the case of a periodic perturbation. Then a periodic sequence of alternating spikes and troughs develops. We propose a hypothesis that for a broad class of initial conditions a singularity develops at the bottom of a trough. Its formation requires a finite time. We have described the basic features of the solution at the end of this time. It is probable that the spatial periodicity of the solutions is not important in connection with the singularity. Specifically, similar phenomena should be observed as well for quasiperiodic and also for spatially localized initial data such that an isolated trough develops. Note that, as mentioned in Sec. 8, these results only hold for initial data which drop off exponentially as a function of the order of the harmonic.

I wish to express my indebtedness to S. I. Anisimov for useful discussions, to the referee for pointing out the need to elucidate questions associated with the short-wavelength instabilities, and especially to A. Yu. Dem'yanov and A. V. Chekhlov for help with the calculations. This work was performed with support from the Russian Fund for Fundamental Research (project number 95-02-06381-a).

¹Membership in the class of initial data admitting vortex collapse, is still the subject of extensive discussion.

²Note that in the extremely nonlinear regime (not treated here) boundary-layer turbulence occurs in this case, which eventually leads to fragmentation of the originally compact mass of liquid.

³The line $U=K$ corresponds to free fall, in which case the effect of pressure is irrelevant.

⁴The change in the velocity U from its initial value U_0 to the value U_b it has when intersection with the bisectrix occurs is small if the trajectory is near the center, $(U_0-U_b)=U_0^2$.

⁵Under the condition, of course, that it starts out from near the equilibrium point.

⁶Crude and precise numerical calculations will be discussed below.

⁷In Refs. 25 and 26 the equation is written in terms of the velocity and amplitude and the integration is carried out over time. In this form it is very involved and the general analysis is hard to do.

⁸Here the cases $g=0$ and $g=1$ (the unstable cases) are referred to. The case of gravitational waves, $g=-1$, requires additional clarification (see below).

⁹With the exceptions noted above regarding the cases $N=1$ and $g=-1$.

¹⁰It is more convenient to display the physical velocity fields themselves and the shape of the boundary separately. This will be done in connection with the comparison with the results of the numerical simulation.

¹E. A. Kuznetsov, M. D. Spector, and V. E. Zakharov, *Phys. Lett. A* **182**, 387 (1993).

²E. A. Kuznetsov, M. D. Spector, and V. E. Zakharov, *Phys. Rev. E* **49**, 1283 (1994).

³L. D. Landau and E. M. Lifshitz, *Fluid Mechanics*, Pergamon Press, Oxford (1987).

⁴V. E. Zakharov, *Zh. Éksp. Teor. Fiz.* **62**, 1745 (1972) [*Sov. Phys. JETP* **35**, 908 (1972)].

⁵S. I. Anisimov, M. A. Berezovskii, M. F. Ivanov, I. V. Petrov, A. M. Rubenchik, and V. E. Zakharov, *Computer Simulation of the Langmuir Collapse*, Preprint No. 167, Inst. of Automation and Electrometry, Novosibirsk (1981).

⁶S. I. Anisimov, M. A. Berezovskii, M. F. Ivanov, I. V. Petrov, A. M. Rubenchik, and V. E. Zakharov, *Phys. Lett. A* **92A**, 32 (1982).

⁷H. Aref, *Phys. Fluids* **22**(3), 393 (1979).

⁸S. G. Chefranov, *Zh. Éksp. Teor. Fiz.* **99**, 1149 (1991) [*Sov. Phys. JETP* **72**, 640 (1991)].

⁹L. W. Schwartz and J. D. Fenton, *Ann. Rev. Fluid Mech.* **14**, 39 (1982).

- ¹⁰S. W. Haan, *Phys. Fluids B* **3**(8), 2349 (1991).
- ¹¹V. B. Ropzanov, J. G. Lebo, S. G. Zaitsev *et al.*, Preprint No. 56, Lebedev Inst. of the Russian Acad. of Sciences, Moscow (1990).
- ¹²S. I. Anisimov, Ya. B. Zel'dovich, N. A. Inogamov, and M. F. Ivanov, in *Shock Waves, Explosions, and Detonations*, J. R. Bowen, J.-C. Leyer, and R. I. Soloukhin (eds.), Progress in Astronautics and Aeronautics Series, Vol. 87, M. Summerfield (editor-in-chief), AIAA, Washington, DC (1983).
- ¹³A. V. Shurunov, A. N. Davydov, V. A. Gal'burt, and E. F. Lebedev, IVTAN Preprint No. 2-157, Moscow (1985).
- ¹⁴A. L. Kuhl, in *Dynamics of Exothermicity*, J. R. Bowen (ed.), Gordon & Breach, Longhorn, PA (1994) (in press).
- ¹⁵A. B. Bud'ko, A. L. Velikovich, M. A. Liberman, and F. S. Felber, *Zh. Éksp. Teor. Fiz.* **96**, 140 (1989) [*Sov. Phys. JETP* **69**, 76 (1989)].
- ¹⁶V. S. Imshennik and D. K. Nadezhdin, in *Progress in Science and Technology*, Astronomy Series, Vol. 21, R. A. Synyaev (ed.), VINITI (1982).
- ¹⁷S. A. Grebenev and R. A. Synyaev, *Pis'ma Astron. Zh.* **13**, 945 (1987) [*Sov. Astron. Lett.* **13**, 397 (1987)].
- ¹⁸D. Arnett, B. Fryxwell, and E. Muller, *Astrophys. J. (Lett.)*, **341**, L63 (1989).
- ¹⁹S. I. Voropayev, Y. D. Afanasyev, and G. J. F. Van Heijst, *Phys. Fluids A* **5**(10), 2461 (1993).
- ²⁰D. H. Sharp, *Physica D* **12D**, 3 (1984).
- ²¹H. J. Kull, *Phys. Rep.* **206**, 197 (1991).
- ²²L. N. Sretenskiĭ, *Theory of Wave Motion in Fluids* [in Russian], Nauka, Moscow (1977).
- ²³R. D. Richtmyer, *Commun. Pure Appl. Math.* **13**, 297 (1960).
- ²⁴E. E. Meshkov, *Izv. Akad. Nauk SSSR, Mekh. Zhidk. Gaza* No. 5, 151 (1969) [*Izv. Akad. Nauk SSSR, Mekh. Zhidk. Gaza* **4**(5), 151 (1969)].
- ²⁵D. Layzer, *Astrophys. J.* **122**, 1 (1955).
- ²⁶H. J. Kull, *Phys. Rev. Lett.* **51**, 1434 (1983).
- ²⁷N. A. Inogamov, *Pis'ma Zh. Tekh. Fiz.* **55**, 505 (1992) [*Sov. Tech. Phys. Lett.* **55**, 521 (1992)].
- ²⁸O. M. Belotserkovskii and Yu. M. Davydov, *PIC Methods in Gasdynamics* [in Russian], Nauka, Moscow (1982).
- ²⁹N. A. Inogamov and A. V. Chekhlov, in *4th Internat. Workshop on the Phys. of Compressible Turbulent Mixing*, P. F. Linden, D. I. Youngs, and S. B. Dalziel (eds.), Cambridge Univ. Press (1993).

Translated by David L. Book